DOI: 10.1002/chem.200900479

A High-Barrier Molecular Balance for Studying Face-to-Face Arene–Arene Interactions in the Solid State and in Solution

Yong S. Chong, William R. Carroll, William G. Burns, Mark D. Smith, and Ken D. Shimizu*[a]

Abstract: An atropisomeric molecular balance was developed to study face-to-face arene–arene interactions. The balance has a large central 1,4,5,8-naphthalene diimide surface that forms intramolecular arene–arene interactions with two pendent arms. The balance adopts distinct *syn* and *anti* isomers with varying numbers of intramolecular interactions. Thus, the strength of the arene–arene interaction could be quantitatively measured by NMR spectroscopy from the *anti*/*syn* ratios. The size of the arene arms was easily varied, which allowed examination of the relationship between arene size and strength of the interaction. A nonlinear size dependence was observed in solution with larger arene arms having a disproportionately stronger arene–arene interaction. The intramolecular arene–arene interactions were also characterized in the solid state by X-ray crystallography. These studies were facilitated by the kinetic stability of the *syn* and *anti* isomers at room temperature due to the high isomerization barrier ($\Delta G = 27.0$ kcal mol^{-1}). Thus, the *anti* isomer could be selectively isolated and crystallized in its folded conformation. The X-ray structures confirmed that the *anti* isomers formed two strong intramolecular arene–arene interactions with face-to-face geometries. The solid-state structure analysis also reveals that the rigid framework may contribute to the observed nonlinear size trend. The acetate linker is slightly too long, which selectively destabilizes the balances with smaller arene arms. The larger arene arms are able to compensate for the longer linker and form effective intramolecular arene–arene interactions.

Keywords: arene–arene interactions · atropisomerism · molecular torsional balance · noncovalent interactions · pi interactions

Introduction

Arene–arene interactions[1,2] play an important role in controlling the structure and reactivity of biological[3] and synthetic molecules[4] and polymers.[5–8] For example, arene–arene interactions assist in directing the folding and assembly of proteins and polynucleotides.[9] Arene–arene interactions have also been used to assemble supramolecular structures[10–12] and to control the stereoselectivity of organic transformations.[13,14] Despite their importance, the factors that govern arene–arene interactions are not well understood, in contrast to other noncovalent interactions such as hydrogen bonding. There are two major reasons: the first is that arene–arene interactions are the sum of multiple forces of similar magnitude such as charge transfer, solvation, electrostatic interactions, and London dispersion forces.[15] Thus, the dominant term will vary depending upon an arene's substituents,[16–19] size,[20] and solvent environment.[21,22] A second difficulty in studying arene–arene interactions is their geometric promiscuity, which arises from the lack of a strong electrostatic polarization in most arene surfaces. Arene surfaces can adopt a variety of geometries with similar stabilities.[23] The most common geometries are shown in Figure 1. In addition to the face-to-face and edge-to-face geometries, there are also a continuum of intermediate geometries.[24–27]

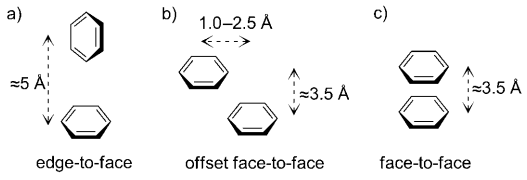

Figure 1. Three general types of arene–arene geometries.

[a] Dr. Y. S. Chong, W. R. Carroll, W. G. Burns, M. D. Smith, Prof. K. D. Shimizu
Department of Chemistry, University of South Carolina
631 Sumter St., Columbia SC 29208 (USA)
Fax: (+1) 803-777-9521
E-mail: shimizu@mail.chem.sc.edu

 © 2009 Wiley-VCH Verlag GmbH & Co. KGaA, Weinheim WILEY InterScience DISCOVER SOMETHING GREAT

Thus, we have designed a new molecular balance **1** (Scheme 1) to study face-to-face arene–arene interactions. The two arene arms of **1** form intramolecular face-to-face

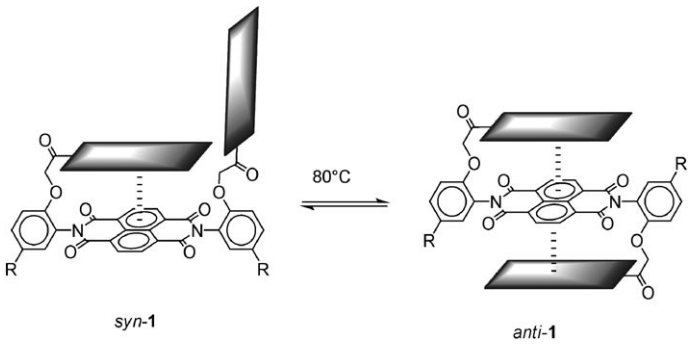

Scheme 1. Schematic representation of molecular balance **1** (R = *tert*-amyl), which is designed to measure face-to-face arene–arene interactions. Restricted rotation around the two C_{aryl}–N_{imide} single bonds leads to room temperature stable *syn* and *anti* isomers that contain one and two intramolecular arene–arene interactions, respectively.

interactions with a large 1,4,5,8-naphthalene diimide surface. In the unfolded *syn* isomer, only one arene arm can form an intramolecular interaction. In the folded *anti* isomer, both arene arms can form intramolecular interactions. Thus, the *anti*/*syn* ratio yields a measure of the arene arm to naphthalene diimide interaction. Molecular balance **1** was efficiently assembled in two steps. Thus, arene arms of varying size from benzene to pyrene could be readily incorporated and their intramolecular interactions measured. We were particularly interested in how the stability of the arene–arene interaction varied with the size of the arene surface. Recently, theoretical studies by Grimme have predicted that the strength of the arene–arene interaction will not scale linearly with arene surface area.[20]

There are a number of advantages in using small-molecule model systems to study weak, noncovalent forces.[4] For example, arene–arene interactions were initially studied in biological systems such as proteins, peptides, and nucleotides.[9,19,28] However, the contributions of individual arene–arene interactions were often difficult to accurately extricate from the myriad of other noncovalent interactions that are present in biological recognition systems.[29,30] Thus, small-molecule model systems have been developed to study arene–arene interactions in simpler and more controlled environments.[2,31] These model systems can be classified as either bimolecular or unimolecular systems, where the noncovalent interactions are inter- or intramolecular. Examples of bimolecular model systems by Rebek[32] and Hunter[33,34] and their groups are shown in Figure 2, where the two interacting arene surfaces are on separate molecules. Hunter's bimolecular model system, in particular, provided conformation of the widely used Hunter–Sanders electrostatic model of the arene–arene interaction.[2] Both systems use supporting hydrogen-bonding interactions to ensure the formation

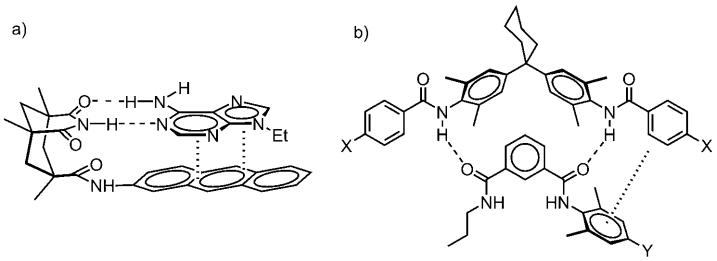

Figure 2. Examples of bimolecular model systems by a) Rebek et al.[32] and b) Hunter et al.[33,34] for measuring the strength of arene–arene interactions.

of bimolecular arene–arene complexes as the arene–arene interaction alone is too weak and nondirectional. This introduces the problem of subtracting out the entropic and enthalpic contributions of these supporting interactions.[35] The hydrogen bonds also limit the analysis of these systems to non-hydrogen bonding organic solvents.

The second class of arene–arene model systems are unimolecular systems that measure intramolecular arene–arene interactions. Unimolecular systems use a rigid covalent framework to bring two arene surfaces together. Thus, unimolecular systems can, in principle, provide better control over the arene–arene geometry and can be studied in a wider range of solvent environments. Examples include Siegel's 1,8-biarylnaphthalenes (Figure 3a),[36] Rashkin–Waters'

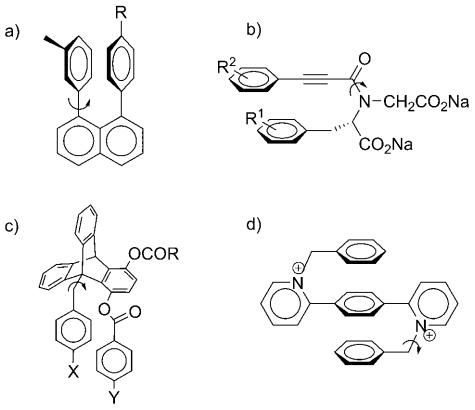

Figure 3. Four unimolecular model systems for studying arene–arene interactions. See text for details.

benzylpyridium,[19] Gellman's propargylic amides (Figure 3b),[37] Gung's triptycenes (Figure 3c),[17,38] and Cammers-Goodwin's three-state benzylpyridinium system (Figure 3d).[39] Each system adopts multiple conformations due to restricted rotation around a single bond. Measurement of the rate of isomerization or the equilibrium ratio yields a measure of the intramolecular arene–arene interaction.

One of the most successful examples of an unimolecular model system is Wilcox's molecular torsional balance, which

 © 2009 Wiley-VCH Verlag GmbH & Co. KGaA, Weinheim

was designed to study edge-to-face arene–arene interactions (Scheme 2).[40] This molecular balance is in equilibrium between *folded* and *unfolded* conformers due to restricted rotation about the C_{aryl}–C_{aryl} bond.[41] In the *folded* conformer,

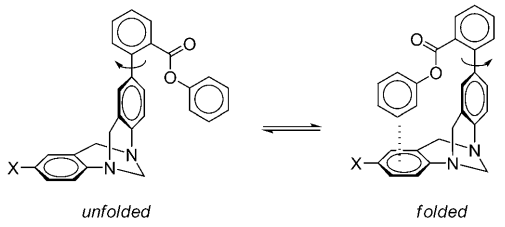

Scheme 2. Wilcox's two-state molecular torsional balance for measuring edge-to-face arene–arene interactions.[42]

the rigid bicyclic framework enforces an intramolecular edge-to-face arene–arene interaction. In the *unfolded* conformer, this edge-to-face interaction is broken. Studies of Wilcox's molecular balance have expanded our understanding of the nature of arene–arene interactions, highlighting the utility of small-molecule model systems. Wilcox's balance has also inspired many computational studies leading to opposing theories on the nature of the arene–arene interactions.[42] Initial computational studies of this system led to the conclusion that dispersion forces are a much stronger component of the edge-to-face interactions than was previously understood.[43] Alternatively, the folding propensities have been attributed to solvent accessibility and the solvophobic effects.[44,45]

Molecular balance **1** incorporates many of the attractive features of Wilcox's balance including a rigid framework and well-defined *folded* and *unfolded* conformations. A key difference is that balance **1** is designed to study face-to-face as opposed to edge-to-face arene–arene interactions. In addition, the analysis of balance **1** is facilitated by the room temperature stability of the *syn* and *anti* isomers.[46–49] In solution, the kinetic stability of the isomers enabled rapid and accurate measurement of the *anti*/*syn* ratios by integrating the ^{1}H NMR spectra as the isomers were in slow exchange. Balance **1** could also be equilibrated in one solvent, and then the *anti*/*syn* ratio measured in another. This was helpful because each balance could be analyzed in its optimal NMR solvent. The kinetic stability of the *anti* and *syn* isomers was also helpful in characterizing the arene–arene interactions of **1** in the solid state. It is often difficult to study intramolecular interactions in the solid state due to the dominance of intermolecular packing forces.[4] Thus, molecular balances often prefer to crystallize in an *unfolded* conformation.[48] In the case of balance **1**, the *syn* and *anti* isomers could be separated and individually crystallized. Of particular interest were the folded *anti* isomers of **1** that contained two symmetrical arene–arene interactions. Crystallization of *anti*-**1b** through *anti*-**1d** and characterization by X-ray crystallography confirmed the presence of face-to-face arene–arene interactions.

Results and Discussion

Synthesis: One of the most attractive features of molecular balance **1** is its efficient two-step synthesis (Scheme 3). This allowed us to rapidly synthesize balances **1a–d** with ben-

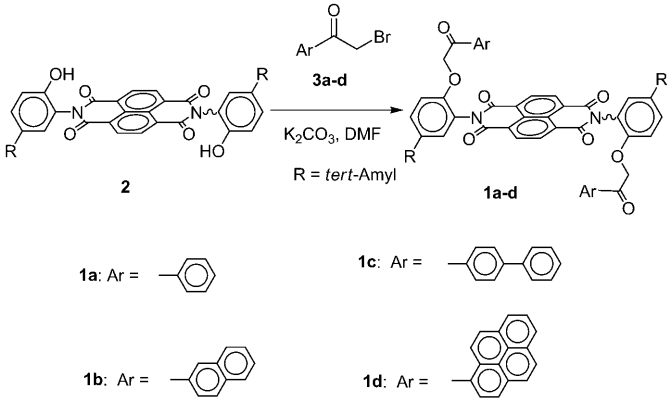

Scheme 3. Synthesis of atropisomeric molecular torsional balances **1a–d** with arene arms of varying size.

zene-, naphthylene-, biphenyl and pyrene arms. First, the bis(phenol) **2** was prepared as previously described through the thermal condensation of two equivalents of 2-amino-4-*tert*-amylphenol with 1,4,5,8-naphthalene diimide.[50] Bis(phenol) **2** was alkylated with an α-bromoacylarene (**3a–d**) under basic conditions to yield balances **1a–d** as a mixture of *syn* and *anti* isomers. The *anti*/*syn* ratios of balances **1a–d** were dependent on the *anti*/*syn* ratio of the starting material, bis(phenol) **2**, which varied greatly due to the low rotational barrier of **2**.[51] Therefore, the crude balances were heated in tetrachloroethane (TCE) at 80 °C for 10 h prior to purification in order to achieve consistent *anti*/*syn* ratios. In the cases of balances **1b** and **1c**, the *syn* isomer was isolated by crystallization. In the case of balance **1d**, the *syn* and *anti* isomers were separated by flash chromatography.

The *syn* and *anti* isomers were assigned by comparison of their NMR spectra with *anti*-enriched samples of **1a–d**, which were prepared by alkylation of *anti*-bis(phenol) **2**. The *anti*-bis(phenol) **2** was prepared as previously described by heating neat samples of bis(phenol) **2** (24 h, 125 °C).[51] The *anti*-enriched balances maintained their *anti*/*syn* ratios (typically >90 % *anti* isomer) as long as they were not heated.

Restricted rotation: In balances **1a–d**, restricted rotation was observed at room temperature. The *syn* and *anti* isomers were in slow exchange with distinct peaks in their ^{1}H NMR spectra. An example is shown in Figure 4 for the biphenyl balance **1c**. The α-keto protons (H_b) and the aromatic naphthalene diimide protons (H_a) were the most clearly resolved in [D_6]benzene (see Figure 4 for assignment). These protons were singlets at room temperature, and thus, could be easily and accurately integrated to mea-

 © 2009 Wiley-VCH Verlag GmbH & Co. KGaA, Weinheim

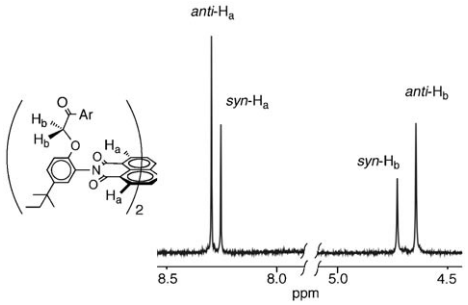

Figure 4. ^{1}H NMR spectrum of **1c** in [D_6]benzene. Distinct signals were observed for *syn*- and *anti*-**1c**, which were in slow exchange at room temperature.

sure the *anti/syn* ratios. Not only were the *syn* and *anti* isomers stable on the NMR timescale, they also were kinetically stable. This was evident from analysis of *anti*-enriched samples of **1**, which maintained steady *anti/syn* ratios for days at room temperature.

The isomerization barrier was measured by heating *anti*-enriched **1** at 80 °C in [D_2]TCE and monitoring the change in the *anti/syn* ratios over the course of several hours by ^{1}H NMR. The isomerization kinetics were consistent with a first order process. A plot of $\ln[(R-R_e)/(R+1)]$ versus time yielded a straight line, where R and R_e are the *anti*/*syn* ratios at time t and at equilibrium, respectively.[52] From the slope of the plot, a first-order rate constant of $2.37\times10^{-4}\,s^{-1}$ was measured for balance **1b**, which equates to an isomerization barrier of 27.0 kcal mol^{-1} calculated with the Eyring equation.[53] The Eyring equation was also used to estimate a half-life of 55 days at 25 °C, which is consistent with the observation that the isomers were stable for extended periods of time at room temperature. However, the barrier was also low enough that the equilibrium *anti*/*syn* ratio could be achieved with gentle heating. To measure the equilibrium *anti*/*syn* ratios, the balances were heated for 10 h at 80 °C. These conditions were chosen because they corresponded to more than ten half-lives and thus, ensured that the balance had reached equilibrium.

***anti/syn* ratios**: The equilibrium *anti*/*syn* ratios provide a measure of the strength of the intramolecular arene–arene interactions in balance **1**. This was evident from the increasing equilibrium *anti*/*syn* ratios with increasing arene surface area (Table 1). In TCE, the lowest ratios were measured for the smallest benzene balance **1a**, which were near unity (45:55). The highest ratios (86:14) were measured for the largest pyrene balance **1d**.

Table 1. The equilibrium *anti*/*syn* ratios and ΔG (kcal mol^{-1}) of balances **1a–d** in DMSO, TCE, and neat. The *anti*/*syn* ratios were measured by integration of the ^{1}H NMR spectra after equilibration of the balances in solution and in the solid states (80 °C, 10 h).

Solvent	**1a**	**1b**	**1c**	**1d**
TCE	45:55	53:47	61:39	86:14
	(+0.13)	(−0.077)	(−0.29)	(−1.2)
DMSO	47:53	55:45	60:40	80:20
	(+0.077)	(−0.13)	(−0.26)	(−0.89)
neat	58:42	52:48	>99:1	>99:1
	(−0.21)	(−0.051)	(>−3.0)	(>−3.0)

Control studies were carried out to rule out other possible influences on the *anti*/*syn* ratios. First, the effect of intermolecular aggregation was assessed by varying the balance concentration from 0.5 mM to 5.0 mM. The *anti*/*syn* ratios of balances **1a–d** remained constant over this concentration range. Second, the influence of the differences in dipole moment of the *syn* and *anti* isomers was examined by equilibration of the balances in dimethyl sulfoxide (DMSO), a more polar solvent. The *anti*/*syn* ratios measured in DMSO were very similar to those obtained in TCE (Table 1). This suggests that the differences in the molecular dipoles of the *syn* and *anti* isomers does not have a strong influence on the *anti*/*syn* ratios. For comparison, we have studied similar *N*,*N*-diarylimide atropisomeric systems where there are large differences in the dipole moments of the *syn* and *anti* isomers.[54] In those cases, the *anti*/*syn* ratios were very sensitive to solvent polarity. The solvent study also helped to eliminate the solvophobic effect as a major contributor to the *anti*/*syn* ratios.[55]

From the *anti*/*syn* ratios, the relative energies ΔG of the intramolecular arene–arene interactions can be quantitatively estimated from Equation (1):

$$\Delta G = -RT\ln([anti]/[syn]) \quad (1)$$

These are shown in Table 1 in parentheses. A plot of the energy of the interaction versus the arene surface area as measured by the number of carbons atoms was nonlinear (Figure 5). The larger arene balances had disproportionately

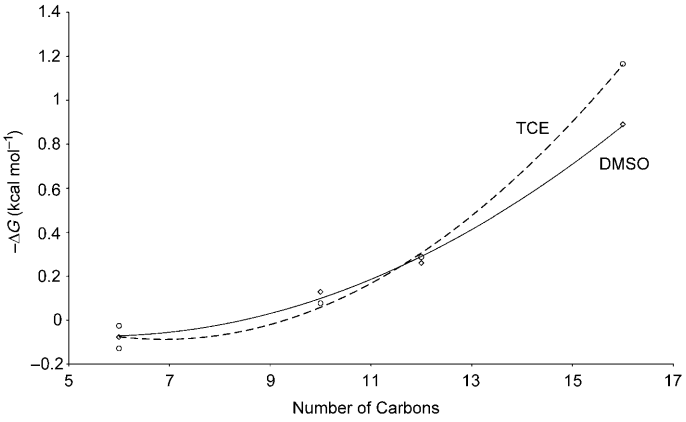

Figure 5. Plot of the $-\Delta G$ (kcal mol^{-1}) of the arene–arene interactions in solution for balances **1a–d** versus size of the arene surfaces as measured by the number of carbons.

stronger arene–arene interactions than the smaller arene balances. This trend is consistent with recent computational studies by Grimme that predicted a similar nonlinear relationship between the magnitude of the arene–arene interaction and the arene size.[20] The origin of this trend was attrib-

 © 2009 Wiley-VCH Verlag GmbH & Co. KGaA, Weinheim

uted to the enhanced dispersion terms of larger, more polarizable arene surfaces.

However, the overall magnitude of the arene–arene interactions in balance **1** was significantly smaller than expected. For example, **1a** with a benzene surface had a very small ΔG of folding, and **1b** with the naphthalene surface has a ΔG of about 0.1 kcal mol^{-1}. For comparison, with other model systems benzene–benzene interactions of $\approx$1.0 kcal mol^{-1} were measured.[38,40,48] There are a number of possible reasons for the low estimates of the arene–arene interactions in **1**. The most important is the elevated equilibration temperatures. Balance **1** was heated to 80 °C in order to reach equilibrium, and thus, the ΔG values in Table 1 are a measure of the arene–arene interaction at these elevated temperatures. In contrast, the higher values for the arene–arene interactions reported for other balance systems were all measured at room temperature or lower temperatures.[38,40,48] Balance **1** could be heated at a lower temperature for a longer period of time. However, this did not change the observed *anti*/*syn* ratios. The reason is that the *anti*/*syn* ratios correspond to equilibrium ratios at the temperature at which the C_{aryl}–N_{imide} bonds stopped rotating and not to the temperature the balance was heated to. A second possible reason is that the arene arms can form attractive interactions in the *syn* conformer. This would reduce the difference in stability between the isomers and lead to an apparently smaller arene–arene interaction. The possibility of repulsive interactions between the arene arms in the *syn* isomer was also considered. However, repulsive interactions were deemed unlikely due to the ability of the *syn* isomer to avoid unfavorable interactions because of the flexibility of the ether linkers. Finally, both interacting arene surfaces in the balances are electron poor, and the Hunter–Sanders electrostatic arene–arene model predicts that these electrostatically similar arene surfaces will form weaker arene–arene interactions.[56] The 1,4,5,8-naphthalene diimide surface is highly electron deficient due to the four imide carbonyl substituents. Likewise, the arene arms of balance **1** are electron poor due to their acetyl linkers.

Solid-state analysis: Next, balance **1** was characterized in the solid state. These studies established that the intramolecular arene–arene interactions were maintained in the solid state. This allowed us to precisely characterize the face-to-face geometry of the arene surfaces by using X-ray crystallography. First, the equilibrium *anti*/*syn* ratios were measured in the solid state (Table 1). The isomerization barriers in the solid state were similar to the isomerization barriers in solution. Thus, the neat balances were equilibrated under similar conditions (10 h at 80 °C). The solids were cooled to room temperature and then dissolved in a NMR solvent and their *anti*/*syn* ratios were measured by integration of the NMR spectra. The measured *anti*/*syn* ratios were qualitatively similar to those obtained in solution, suggesting that the intramolecular arene–arene interactions were maintained in the solid state. The lowest *anti*/*syn* ratios were observed for the smaller arene surfaces (**1a** and **1b**), and the highest *anti*/*syn* ratios were observed for the larger arene surfaces (**1c** and **1d**). However, the changes in ratio were very abrupt as the *anti*/*syn* ratios were either about 50:50 or 99:1. This suggests that a combination of intramolecular and intermolecular (packing effects) interactions were operative in the solid state.

Crystallographic studies allowed us to measure and compare the geometries and orientations of the intramolecular arene–arene interactions in balances **1b–d**. These analyses were facilitated by the room temperature stability of the *syn* and *anti* isomers. Studies of conformationally flexible molecules have often been hampered by the inability to selectively crystallize the folded conformer of interest, as intermolecular interactions often dominate in the solid state. However, in the case of balance **1**, the folded *anti* isomer is kinetically stable and thus, could be separated from the *syn* isomer and selectively crystallized. X-ray quality crystals of *anti* isomers of balances with naphthalene (**1b**), biphenyl (**1c**), and pyrene arms (**1d)** were obtained. In each case, the expected intramolecular arene–arene interactions were observed (Figure 6). Both arene arms form symmetrical face-to-face

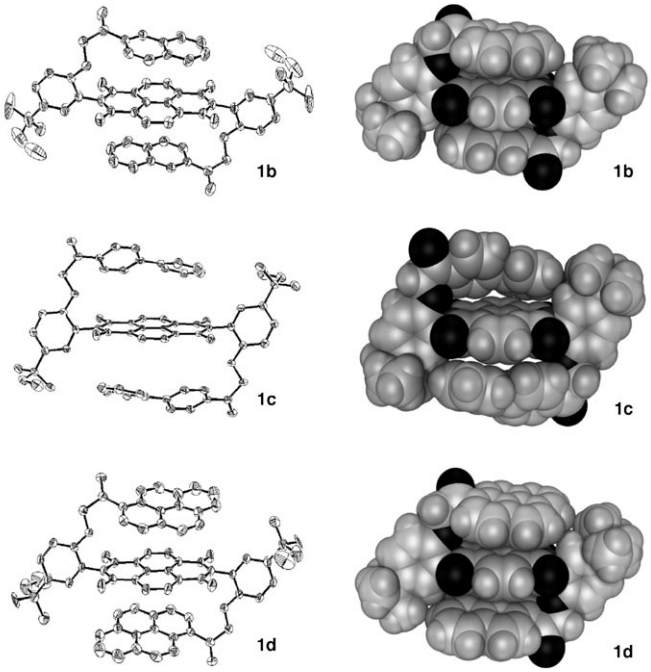

Figure 6. X-ray crystal structures of *anti*-**1b**, **1c**, and **1d** in ORTEP (left) and space filling depictions (right). The hydrogens are not shown in the ORTEP figures for viewing clarity.

arene–arene interactions above and below the central naphthalene diimide surface. The inability to crystallize the benzene balance **1a** maybe due to the weak intramolecular arene–arene interactions in **1a**.

The relative orientations of the interacting arene surfaces in **1b** thru **1d** are shown in Figure 7. The arene arms are shown in black and the naphthalene diimide surfaces are shown in gray. The individual rings of the arene arm are la-

 © 2009 Wiley-VCH Verlag GmbH & Co. KGaA, Weinheim

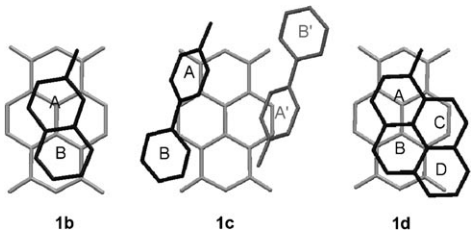

Figure 7. Top view of the intramolecular arene–arene interactions in the X-ray crystal structures of *anti*-**1b**, *anti*-**1c**, and *anti*-**1d**. The 1,4,5,8-naphthalene diimide surface is shown in gray and the top arene arm is shown in black. The second arene arm is not shown because its orientation is identical to the first arene arm. In the case of *anti*-**1d**, the biphenyl arene arm from an adjacent molecule is shown in black.

beled A thru D. Only one arene arm is shown for each balance as the two arms are symmetrically positioned above and below the central naphthalene diimide surface. The naphthalene and pyrene arms (**1b** and **1d**) show a strong face-to-face interaction having almost maximal surface overlap with the naphthalene diimide surface. The relative positioning of the naphthalene and pyrene surfaces is almost identical. The A and B rings of the pyrene in **1d** are almost super-imposable with the corresponding A and B rings of the naphthalene in **1b**. The arene–arene geometry in **1b** is also virtually identical to that of a crystal structure reported by Hamilton et al. of the same two surfaces.[57] This suggests that the acetyl linker in balance **1** holds the arene surfaces together with a minimum of steric strain.

The influences of intermolecular packing interactions are more evident in the X-ray structure of balance *anti*-**1c**. The solid-state structure of *anti*-**1c** still maintains a symmetrical folded structure with the two biphenyl arms stacked above and below the central naphthalene diimide surface. However, one biphenyl arm was positioned over the edge and not the center of the naphthalene diimide. This is due to the influence of intermolecular interactions with a second biphenyl arm from an adjacent molecule (shown in gray), which is stacked over the opposing edge of the naphthalene diimide surface (Figure 7). Thus, each naphthalene diimide surface in **1c** interacts with four arene arms. The two biphenyl arms also form intermolecular edge-to-face arene–arene interactions with each other. Although both intra- and intermolecular arene–arene interactions are present in the solid-state structure of **1c**, this is probably not representative of the solution structure. Dilution studies confirmed that intermolecular interactions do not influence the *anti*/*syn* ratios in solution. Overall, the solid-state structures of balances **1b–d** demonstrate that intermolecular arene–arene interactions between the arene arms and the central naphthalene diimide surface are reasonable structures and provide valuable insight into the possible geometries of these interactions.

To study the origins of the solid-state arene–arene geometries, the HOMOs/LUMOs and electrostatic potentials of the respective arene surfaces were calculated by using SPARTAN[58] at a semi-empirical level (AM1). Both of these analyses have been used to rationalized observed arene–arene geometries.[21,59–61] First, the HOMOs of the electron-rich arene arms were calculated, and their interactions with the LUMOs of the electron-poor 1,4,5,8-naphthalene diimide surface were examined (Figure 8). When the

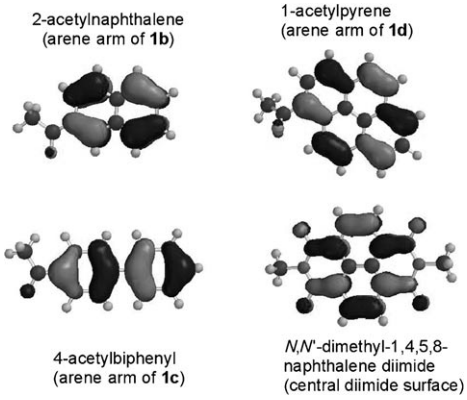

Figure 8. The calculated HOMOs of the arene arms **1b** (top left), **1c** (bottom left), **1d** (top right), and the LUMO of the 1,4,5,8-naphthalene diime (bottom right). Calculations were preformed by using SPARTAN at the semi-empirical level (AM1).[58]

HOMOs and LUMOs are fixed in the orientations observed in the crystal structures of **1c** and **1d**, they show poor phase complementarity. For example, **1b** and **1d** have similar orientations of their arene arms in the solid state. However, the HOMOs of the A and B rings of the naphthalene and pyrene arms of **1b** and **1d** are neither in phase with each other nor are they complementary with the LUMO of the naphthalene diimide surface.

The observed arene–arene orientations in **1b**, **1c**, and **1d** show better correlation with the electrostatic surface potentials of the arene surfaces (Figure 9). The electron-rich regions are highlighted in red and electron-poor regions are highlighted in blue. The most electron-rich region of the

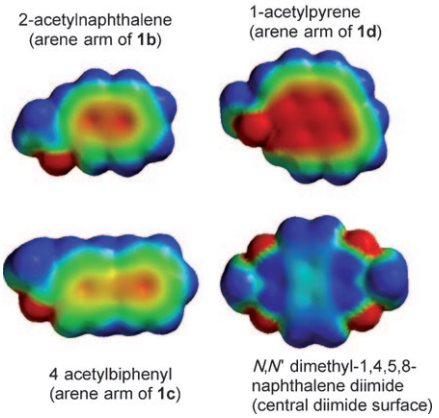

Figure 9. Electrostatic potential surfaces of the arene arms of **1b**, **1c**, and **1d** and the central 1,4,5,8-naphthalene diimide surface (bottom right) calculated by using SPARTAN at a semi-empirical level (AM1).[58] The electron-rich regions are highlighted in red and electron-poor regions are highlighted in blue.

 © 2009 Wiley-VCH Verlag GmbH & Co. KGaA, Weinheim

three arene arms is the center of each surface. The most electron-poor regions of the naphthalene diimide are over the carbonyl carbons and the aromatic C–H groups. The arene–arene orientations observed in balances **1b–d** appear to yield optimal overlap between the electron-rich regions of the arene arms and the electron-poor regions of the naphthalene diimide surface. For example, the folded structure of *anti*-**1d** maximizes the interaction between the electron-rich center of the pyrene surface and the electron-poor naphthalene diimide surface. Similarly, the off-set geometry in biphenyl balance **1c** places the electron-rich centers of the biphenyl surfaces over the electron-poor edges of the naphthalene diimide surfaces. This correlation between geometry and electrostatic complementarity is consistent with Iverson et al.'s analysis of the geometry of the arene–arene complex of 1,4,5,8-naphthalene diimide and naphthalene surfaces.[21]

Comparison of the potential surfaces of the arene arms also provided an electrostatic basis for the stronger intramolecular interactions in pyrene balance **1d**. First, the pyrene surface is significantly more electron-rich than either the naphthalene or biphenyl surfaces, leading to stronger electrostatic or dispersion interactions with the electron-poor naphthalene diimide surface. This is evident from the large red regions of the 1-acetylpyrene in comparison to the 2-acetylnaphthalene or 4-acetylbiphenyl potential surfaces (Figure 9). The lower ionization potential of the pyrene arm appears to be primarily due to its larger, more polarizable surface.[20] A second factor that differentiates the pyrene arm from the other arene arms is the influence of the electron-withdrawing acyl tether. In the case of the naphthalene and biphenyl surfaces, molecular modeling predicts that the acetyl group will be nearly coplanar with the arene surface. This conformation maximizes the electron-withdrawing influence of the acyl group and reduces the electron-donating ability of these smaller arene surfaces. However, in the case of the pyrene surface, the acetyl group is twisted out of conjugation with the arene surface due to the steric interactions between the carbonyl oxygen and the pyrene C_{10} proton. This deplanarization reduces the electron-withdrawing effect of the acetyl tether making the pyrene arm considerably more electron-rich than the other arene arms. The twisted configuration of the pyrene arm was confirmed by examination of the X-ray structures. In pyrene balance *anti*-**1d**, the acetyl group was twisted 39.3° out of the arene plane. In contrast, the acetyl groups in *anti*-**1b** and *anti*-**1c** were twisted only 23.4° and 26.3° out of plane.

Arene–arene distances: Finally, the intramolecular arene–arene distances in the crystal structures provide an additional explanation for the stronger arene–arene interaction observed for pyrene balance **1d**. This analysis suggests that the acyl tether is slightly too long, which destabilizes the folding of the smaller arene balances. The effects are subtle and difficult to see in the side views of the balances shown in Figure 6. However, comparison of the intramolecular centroid-to-plane distances between the individual rings of the arene arms and the naphthalene diimide surfaces clearly shows the influence of the tether length (Table 2). The distances for rings adjacent to the tether are slightly beyond the optimal stacking distances of 3.5 Å (Figure 10). Rings further from the tether have shorter distances (<3.5 Å) and therefore form stronger arene–arene interactions. For example, the ring attached to the tether (A ring) in naphthalene balance **1b** is 3.67 Å from the plane of the naphthalene diimide surface, and the ring furthest from the tether (B ring) has a distance of 3.46 Å. Thus, the larger arene arms can form stronger arene–arene interactions because the rings further from the tether can form more effective arene–arene interactions. This may also explain why the overall magnitudes of the arene–arene interactions were relatively small compared to other balance systems. For example, balance **1a** with only a single ring (A ring) cannot form effective intramolecular arene–arene interactions. This may explain the inability to crystallize *anti*-**1a** as it would not prefer a folded structure.

Table 2. Centroid to plane distances [Å] between the individual rings of the arene arms and the 1,4,5,8-naphthalene diimide surface in the crystal structures of balances **1b**, **1c**, and **1d**. The rings of the arene arms are assigned as A, B, C, and D as shown in Figure 7.

Ring	A	B	C	D
1b	3.67	3.46	–	–
1c	4.16	3.31	–	–
	4.37[a]	5.21[b]		
1d	3.79	3.55	3.78	3.93

[a] Ring A′. [b] Ring B′.

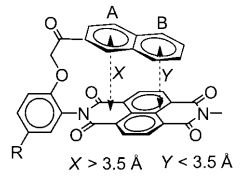

Figure 10. A representation of the correlation between arene arm length and the observed distance to the plane of the 1,4,5,8-naphthalene diimide.

Conclusions

In summary, we have successfully synthesized four new molecular balances for studying face-to-face arene–arene interactions. Due to their efficient syntheses, balances with arene arms of varying size (benzene, naphthalene, biphenyl, and pyrene) could be readily prepared and studied. The balances adopt distinct *syn* and *anti* isomers that have differing numbers of intramolecular arene–arene interactions. Therefore, the *anti*/*syn* ratio provides a measure of the intramolecular arene–arene interactions. A unique feature of these balances was the kinetic stability of their *syn* and *anti* isomers at room temperature. This stability facilitated the accurate measurement of the strength of the arene–arene interactions in solution and also the conformational analysis of the arene–arene interaction in the solid state. First, the *syn* and *anti* isomers were in slow exchange and thus, the *anti*/*syn* ratio could be readily measured by integration of the ^{1}H NMR spectra. Second, the stability of the isomers en-

 © 2009 Wiley-VCH Verlag GmbH & Co. KGaA, Weinheim

abled the selective crystallization of *anti*-**1**, which maintained its folded structure in the solid state. Thus, the distances and orientations of the arene surfaces could be precisely analyzed by X-ray crystallography.

A strong nonlinear free-energy trend was observed in solution. Larger arene surfaces (pyrene: **1d**, and biphenyl: **1c**) formed disproportionately stronger arene–arene interactions than smaller surfaces (benzene: **1a**, and naphthyl: **1b**). These results are in agreement with the recent calculations, which predict that larger arene surfaces form stronger arene–arene interactions due to their greater polarizability.[20] However, a more careful structural and computational analysis identified additional contributing factors. Specifically, the acyl tether connecting the interacting arene surfaces imposes conformational constraints and electrostatic influences that contribute to the observed nonlinear trends. This study demonstrates that even in simple model systems, the study of weak, noncovalent interactions is still very challenging.[43]

Experimental Section

General methods: ^{1}H NMR and ^{13}C NMR spectra were obtained by using a Varian Mercury 300 MHz NMR spectrometer and a Varian Mercury 400 MHz NMR spectrometer. Peak areas were determined by using the standard deconvolution routine in Varian VNMR 6.1B software. Visual inspection of the difference mode spectra (simulation/data) was used to test fit. Infrared spectra were performed on a Perkin–Elmer 1600 series FT-IR spectrometer by using sodium chloride plates. Mass spectra were performed on a Finnigan 4521C system by using a GC probe for volatile samples and a solid probe for nonvolatile samples. High resolution mass spectroscopy (HRMS) was performed on a VG 705Q spectrometer. All reagents were purchased from either Aldrich or Acros and used as received. Elemental analysis was preformed by Atlantic Microlabs, Inc. The crystallographic data were collected on a Bruker SMART APEX CCD-based diffractometer system ($Mo_{K\alpha}$ radiation, λ = 0.71073 Å). CCDC-720864 (*anti*-**1b**), CCDC-720863 (*anti*-**1c**), and CCDC-720865 (*anti*-**1d**) contain the supplementary crystallographic data for this paper. These data can be obtained free of charge from The Cambridge Crystallographic Data Centre via www.ccdc.cam.ac.uk/data_request/cif

Quantification of the *anti/syn*-ratio: The ^{1}H NMR spectra of balances **1a–d** in [D_2]TCE showed two singlets in the δ = 4–6 ppm region. These were assigned to the methylene protons of the acetyl linker of the *syn* and *anti* isomers. The more upfield singlet was assigned to the *anti* isomer by comparison with the ^{1}H NMR of *anti*-enriched samples. The relative magnitude of each singlet was quantified by integration by using the peak fitting commands in the Varian VNMRJ software.

Bis(phenol) 2: *anti*/*syn*-Bis(phenol) **2** and *anti*-enriched bis(phenol) **2** were prepared as previously described.[50,51] In brief, a solution of 1,4,5,8-naphthalenetetracarboxylic dianhydride (250 mg, 0.932 mmol) and 2-amino-4-*tert*-amylphenol (345 mg, 3.16 mmol) in glacial acetic acid (8 mL) was heated at reflux for 2.5 h. The resulting light brown precipitate was separated through filtration and dried in vacuo to give *anti*/*syn*-**2** (540 mg, 99%). *anti*-Enriched bis(phenol) **2** was prepared by heating a neat sample of *anti*/*syn*-**2** at 110°C for 10 h. The sample was cooled to room temperature. ^{1}H NMR ([D_6]acetone) verified that the samples were >95% *anti*-**2**. The *anti*-enriched samples were stable at room temperature in the solid state but isomerized rapidly in solution ($t_{1/2} \approx 13$ min).

Benzene balance 1a: A solution of bis(phenol) **2** (110 mg, 0.186 mmol), potassium carbonate (257 mg, 1.86 mmol) and 2-bromoacetophenone (79.4 mg, 0.391 mmol) in dry DMF (5 mL) was stirred at room temperature for 6 h. The reaction mixture was added to a solution of 1 N HCl (25 mL) resulting in the formation of a precipitate. The precipitate was separated through filtration and dried in vacuo to give crude compound **1a**. The crude product was heated in TCE at 80°C for 10 h, yielding **1a** as a light brown solid (130 mg, 84%) with an *anti*/*syn* ratio of 45:55. ^{1}H NMR (300 MHz, $CDCl_3$, 25°C, TMS): δ = 8.75 (s, 4H-*anti*), 8.74 (s, 4H-*syn*), 7.80–7.74 (m, 4H-*anti* and 4H-*syn*), 7.45–7.16 (m, 10H-*anti* and 10H-*syn*), 7.05 (d, J = 8.8 Hz, 2H-*syn*), 7.03 (d, J = 8.8 Hz, 2H-*anti*), 5.18 (s, 4H-*anti* and 4H-*syn*), 1.66 (q, J = 7.4 Hz, 4H-*anti* and 4H-*syn*), 1.32 (s, 12H-*anti*), 1.31 (s, 12H-*syn*), 0.77 ppm (t, J = 7.4 Hz, 6H-*anti* and 6H-*syn*); ^{13}C NMR (125 MHz,$CDCl_3$, 25°C, TMS): δ = 194.1, 162.7, 151.2, 143.8, 134.5, 133.4, 131.1, 131.0, 128.5, 128.4, 128.1, 128.0, 127.8, 127.3, 126.9, 123.6, 133.4, 72.1, 72.0, 37.6, 37.0, 28.4, 9.2 ppm; IR (liquid film): $\tilde{\nu}$ = 697, 734, 767, 825, 982, 1127, 1198, 1224, 1249, 1346, 1448, 1508, 1582, 1604, 1679, 1716, 2963, 3058 cm^{-1}; HRMS (ESI) m/z: calcd for $[M+H]^+$: $C_{52}H_{46}N_2O_8$ 826.3254; found 826.3268.

Naphthalene balance 1b: A solution of bis(phenol) **2** (400 mg, 0.677 mmol), potassium carbonate (934 mg, 6.77 mmol), and α-bromo-2′acetonaphthone (361 mg, 1.42 mmol) in dry DMF (15 mL) was stirred for 12 h. The reaction mixture was added to a solution of 1 N HCl (25 mL) resulting in the formation of a precipitate. The precipitate was separated through filtration and dried in vacuo to give crude compound **1b**. The crude product was heated in TCE at 80°C for 10 h, yielding **1b** as a light brown solid (535 mg, 85%) with an *anti*/*syn* ratio of 53:47. ^{1}H NMR (300 MHz, $CDCl_3$, 25°C): δ = 8.07 (s, 4H-*anti* and 4H-*syn*), 7.77 (dd, J = 8.5, 1.6 Hz, 2H-*syn*), 7.71 (dd, J = 8.5, 1.6 Hz, 2H-*anti*), 7.58 (d, J = 2.5 Hz, 2H-*syn*), 7.42 (d, J = 2.5 Hz, 2H-*anti*), 7.36–7.01 (m, 14H-*anti* and 14H-*syn*), 6.76 (d, J = 8.8 Hz, 2H-*syn*), 6.72 (d, J = 8.8 Hz, 2H-*anti*), 4.83 (s, 4H-*syn*), 4.70 (s, 4H-*anti*), 1.65 (q, J = 7.4 Hz, 4H-*syn*), 1.57 (q, J = 7.4 Hz, 4H-*anti*), 1.31 (s, 12H-*syn*), 1.22 (s, 12H-*anti*), 0.85 (t, J = 7.4 Hz, 6H-*syn*), 0.79 ppm (t, J = 7.4 Hz, 6H-*anti*); ^{13}C NMR (125 MHz,$CDCl_3$, 25°C): δ = 195.0, 194.8, 162.4, 151.3, 151.1, 143.9, 135.2, 135.0, 132.2, 132.1, 132.0, 131.8, 130.6, 130.5, 130.3, 129.3, 128.8, 128.1, 128.0, 127.8, 127.6, 127.4, 126.9, 126.5, 126.3, 126.1, 123.9, 123.8, 123.5, 113.7, 113.5, 77.3, 77.0, 76.7, 72.9, 72.8, 37.6, 37.6, 37.1, 37.0, 28.4, 9.2, 9.1; FTIR (film): $\tilde{\nu}$ = 2963, 2927, 1714, 1678, 1626, 1582, 1508, 1469, 1446, 1346, 1250, 1191, 1125, 979, 822, 769, 757, 475 cm^{-1}; HRMS (ESI) m/z: calcd for $[M+H]^+$: $C_{60}H_{50}N_2O_8$: 926.3567; found: 926.3585; elemental analysis calcd (%) for $C_{60}H_{50}N_2O_8 \cdot H_2O$: C 76.25, H 5.55, N 2.96. found: C 76.15, H 5.40, N 2.94.

Biphenyl balance 1c: A solution of bis(phenol) **2** (250 mg, 0.423 mmol), potassium carbonate (584 mg, 4.23 mmol), and 2-bromo-4-phenylacetophenone (237 mg, 0.846 mmol) in dry DMF (10 mL) was stirred at room temperature for 12 h. The reaction mixture was added to a solution of 1 N HCl (25 mL) resulting in the formation of a precipitate. The precipitate was separated through filtration and dried in vacuo to give crude **1c**. The crude product was heated in TCE at 80°C for 10 h, yielding **1c** as a light brown solid (410 mg, 99%) with an *anti*/*syn* ratio of 61:39. ^{1}H NMR (300 MHz, $CDCl_3$, 25°C): δ = 8.64 (s, 4H-*anti*), 8.63 (s, 4H-*syn*), 7.87 (dd, J = 8.5, 2.7 Hz, 4H-*anti* and 4H-*syn*), 7.60 (d, J = 8.2 Hz, 4H-*anti* and 4H-*syn*), 7.55–7.35 (m, 14H-*anti* and 14H-*syn*), 7.18 (d, J = 8.8 Hz, 2H-*anti* and 2H-*syn*), 5.44 (s, 4H-*syn*), 5.43 (s, 4H-*anti*), 1.64 (q, J = 7.1 Hz, 4H-*anti*), 1.61 (q, J = 6.6 Hz, 4H-*syn*), 1.29 (s, 12H-*anti*), 1.26 (s, 12H-*syn*), 0.72 (t, J = 7.1 Hz, 6H-*anti*), 0.70 ppm (t, J = 7.4 Hz, 6H-*syn*); ^{13}C NMR (125 MHz, $CDCl_3$, 25°C): δ = 194.3, 162.4, 151.1, 145.5, 143.8, 139.1, 133.3, 130.9, 129.0, 128.9, 128.5, 128.1, 127.8, 126.9, 126.8, 126.7, 123.5, 113.4, 72.3, 37.6, 37.0, 28.4, 9.2; IR (film): $\tilde{\nu}$ = 2965, 2357, 1716, 1683, 1604, 1582, 1506, 1448, 1346, 1249, 1210, 766, 730, 698, 668 cm^{-1}; HRMS (ESI) m/z: calcd for $[M+H]^+$: $C_{64}H_{54}N_2O_8$: 978.3880; found 978.3842; elemental analysis calcd (%) for $C_{64}H_{54}N_2O_8 \cdot H_2O$: C 77.09, H 5.66, N 2.81; found C 77.30, H 5.71, N 2.86.

Pyrene balance 1d: A solution of bis(phenol) **2** (100 mg, 0.169 mmol), potassium carbonate (234 mg, 1.69 mmol), and 1-bromoacetylpyrene (112 mg, 0.349 mmol) in dry DMF (5 mL) was stirred at room temperature for 2 h. The reaction mixture was added to a solution of 1 N HCl (25 mL) resulting in the formation of a precipitate. The precipitate was separated through filtration and dried in vacuo to give crude compound **1c** as a red solid (165 mg, 91%) with an *anti*/*syn* ratio of 86:14. The

 © 2009 Wiley-VCH Verlag GmbH & Co. KGaA, Weinheim

crude products were purified and separated from each other by flash chromatography on silica gel (EtOAc/Hex/CH_2Cl_2 1:4:5) to give *syn*-**1d** and *anti*-**1d** as red solids. *syn*-**1d**: ^{1}H NMR (400 MHz, $CDCl_3$, 25 °C): δ = 8.56 (d, J = 8.5 Hz, 2H), 8.19 (d, J = 7.5 Hz, 2H), 8.06 (d, J = 6.8 Hz, 2H), 8.04 (d, J = 8.8 Hz, 2H), 7.98 (d, J = 7.9 Hz, 2H), 7.97 (t, J = 7.8 Hz, 2H), 7.90 (d, J = 9.5 Hz, 2H), 7.75 (s, 4H), 7.47–7.43 (m, 4H), 7.33 (d, J = 8.1 Hz, 2H), 7.15 (d, J = 8.8 Hz, 2H), 7.08 (d, J = 2.4 Hz, 2H), 5.44 (s, 4H), 1.61 (q, J = 7.4 Hz, 4H), 1.26 (s, 12H), 0.73 ppm (t, J = 7.4 Hz, 6H); ^{13}C NMR (125 MHz,$CDCl_3$, 25 °C): δ = 199.6, 162.0, 151.2, 143.7, 133.3, 130.7, 130.1, 129.7, 129.6, 129.5, 128.1, 127.8, 126.8, 126.7, 126.6, 126.2, 125.9, 125.7, 124.2, 123.6, 123.3, 73.5, 37.5, 37.0, 28.4, 9.1 ppm; IR (film): $\tilde{\nu}$ = 2961, 2928, 2923, 2916, 2857, 2852, 2849, 2369, 2362, 2358, 2340, 1712, 1678, 1594, 1582, 1510, 1448, 1443, 1344, 1248, 1105, 846, 768, 669 cm^{-1}; HRMS (ESI) m/z: calcd for $[M+H]^+$: $C_{72}H_{54}N_2O_8$: 1074.3880; found 1074.3906; elemental analysis calcd (%) for $C_{72}H_{56}N_2O_8$: C 80.28, H 5.24, N 2.60; found C 79.87, H 5.15, N 2.31. *anti*-**1d**: ^{1}H NMR (400 MHz, $CDCl_3$, 25 °C): δ = 8.02 (d, J = 9.2 Hz, 2H), 7.92 (d, J = 7.1 Hz, 2H), 7.89 (d, J = 7.1 Hz, 2H), 7.82 (t, J = 7.4 Hz, 2H), 7.75 (d, J = 7.9 Hz, 2H), 7.70 (d, J = 9.3 Hz, 2H), 7.66 (d, J = 8.8 Hz, 2H), 7.54 (dd, J = 8.6, 2.2 Hz, 2H), 7.47 (d, J = 2.2 Hz, 2H), 7.27 (d, J = 8.1 Hz, 2H), 7.25 (d, J = 7.1 Hz, 2H), 7.17 (s, 4H), 7.12 (d, J = 8.8 Hz, 2H), 5.12 (s, 4H), 1.81 (q, J = 7.3 Hz, 4H), 1.48 (s, 12H), 0.91 ppm (t, J = 7.3 Hz, 6H); ^{13}C NMR (125 MHz,$CDCl_3$, 25 °C): δ = 201.1, 161.4, 150.6, 143.6, 132.1, 131.2, 129.9, 129.7, 128.8, 128.5, 128.3, 128.2, 128.1, 127.3, 126.7, 126.4, 126.1, 126.0, 124.1, 123.8, 123.5, 123.2, 123.0, 112.9, 73.5, 37.7, 37.3, 30.9, 29.7, 28.6, 9.3 ppm; IR (film): $\tilde{\nu}$ = 2961, 2928, 2923, 2916, 2857, 2852, 2849, 2369, 2362, 2358, 2340, 1712, 1678, 1594, 1582, 1510, 1448, 1443, 1344, 1248, 1105, 846, 768, 669 cm^{-1}; HRMS (ESI) m/z: calcd for $[M+H]^+$: $C_{72}H_{54}N_2O_8$: 1074.3880; found 1074.3906; elemental analysis calcd (%) for $C_{72}H_{56}N_2O_8$: C 80.28, H 5.24, N 2.60; found C 79.87, H 5.15, N 2.31.

Measurement of the isomerization barrier: The isomerization barrier was calculated from the experimentally measured isomerization rate constant as previously described by using the Eyring equation.[53] The rate of isomerization was determined for balance system **1b**. A sample of *anti*-enriched **1b** (>90% *anti*) was heated at 80 °C in [D_2]TCE and the *anti*/*syn* ratio was monitored by integration of the α-keto protons of the acetyl tether. The first-order rate constant was calculated from the slope of the plot of $\ln[(R-R_e)/(R+1)]$ versus time., where R and R_e are the *anti*/*syn* ratios at time t and at equilibrium, respectively.[52]

Acknowledgements

The authors would like to acknowledge the support of the National Science Foundation (grant 0616442).

[1] E. Meyer, R. Castellano, F. Diederich, *Angew. Chem.* **2003**, *115*, 1244–1287; *Angew. Chem. Int. Ed.* **2003**, *42*, 1210–1250.
[2] C. Hunter, K. Lawson, J. Perkins, C. Urch, *J. Chem. Soc. Perkin Trans. 2* **2001**, 651–669.
[3] P. Chakrabarti, R. Bhattacharyya, *Prog. Biophys. Mol. Biol.* **2007**, *95*, 83–137.
[4] W. Jennings, B. Farrell, J. Malone, *Acc. Chem. Res.* **2001**, *34*, 885–894.
[5] H. Colquhoun, Z. Zhu, C. Cardin, Y. Gan, M. Drew, *J. Am. Chem. Soc.* **2007**, *129*, 16163–16174.
[6] F. Ilhan, M. Gray, K. Blanchette, V. M. Rotello, *Macromolecules* **1999**, *32*, 6159–6162.
[7] U. H. F. Bunz, V. Enkelmann, L. Kloppenburg, D. Jones, K. D. Shimizu, J. B. Claridge, H. C. Zur Loye, G. Lieser, *Chem. Mater.* **1999**, *11*, 1416–1424.
[8] S. Lahiri, J. L. Thompson, J. S. Moore, *J. Am. Chem. Soc.* **2000**, *122*, 11315–11319.
[9] S. Burley, G. Petsko, *Science* **1985**, *229*, 23–28.
[10] D. Venkataraman, S. Lee, J. Zhang, J. S. Moore, *Nature* **1994**, *371*, 591.
[11] M. Nishio, *CrystEngComm* **2004**, *6*, 130–158.
[12] F. Klärner, B. Kahlert, *Acc. Chem. Res.* **2003**, *36*, 919–932.
[13] G. Jones, *Tetrahedron* **2001**, *57*, 7999–8016.
[14] J. García Ruano, J. Aleman, I. Alonso, A. Parra, V. Marcos, J. Aguirre, *Chem. Eur. J.* **2007**, *13*, 6179–6195.
[15] S. Tsuzuki, T. Uchimaru, *Curr. Org. Chem.* **2006**, *10*, 745–762.
[16] S. Arnstein, C. Sherrill, *Phys. Chem. Chem. Phys.* **2008**, *10*, 2646–2655.
[17] B. Gung, X. Xue, Y. Zou, *J. Org. Chem.* **2007**, *72*, 2469–2475.
[18] S. Cockroft, J. Perkins, C. Zonta, H. Adams, S. Spey, C. M. R. Low, J. Vinter, K. Lawson, C. J. Urch, C. Hunter, *Org. Biomol. Chem.* **2007**, *5*, 1062–1080.
[19] M. Rashkin, M. Waters, *J. Am. Chem. Soc.* **2002**, *124*, 1860–1861.
[20] S. Grimme, *Angew. Chem.* **2008**, *120*, 3478–3483; *Angew. Chem. Int. Ed.* **2008**, *47*, 3430–3434.
[21] M. Cubberley, B. Iverson, *J. Am. Chem. Soc.* **2001**, *123*, 7560–7563.
[22] D. Smithrud, T. Wyman, F. Diederich, *J. Am. Chem. Soc.* **1991**, *113*, 5420–5426.
[23] S. K. Burley, G. A. Petsko, *J. Am. Chem. Soc.* **1988**, *110*, 7995.
[24] T. Blundell, J. Singh, J. Thornton, S. Burley, G. Petsko, *Science* **1986**, *234*, 1005–1005.
[25] W. Liu, Y. Jiang, *J. Org. Chem.* **2008**, *73*, 1124–1127.
[26] S. Tsuzuki, K. Honda, T. Uchimaru, M. Mikami, K. Tanabe, *J. Am. Chem. Soc.* **2002**, *124*, 104–112.
[27] M. Sinnokrot, C. Sherrill, *J. Phys. Chem. A* **2006**, *110*, 10656–10668.
[28] M. S. Searle, D. Williams, *Nucleic Acids Res.* **1993**, *21*, 2051–2056.
[29] D. Williams, E. Stephens, D. O'Brien, M. Zhou, *Angew. Chem.***2004**, *116*, 6596–6616; *Angew. Chem. Int. Ed.* **2004**, *43*, 6760–6782.
[30] S. Cockroft, C. Hunter, *Chem. Soc. Rev.* **2007**, *36*, 172–188.
[31] R. M. Hughes, M. L. Waters, *Curr. Opin. Struct. Biol.* **2006**, *16*, 514–524.
[32] J. Rebek, Jr., *Angew. Chem.* **1990**, *102*, 261–272; *Angew. Chem. Int. Ed. Engl.* **1990**, *29*, 245–255.
[33] H. Adams, K. Harris, G. Hembury, C. A. Hunter, D. Livingstone, J. F. Mccabe, *Chem. Commun.* **1996**, 2531–2532.
[34] H. Adams, F. Carver, C. Hunter, J. Morales, E. Seward, *Angew. Chem.* **1996**, *108*, 1628–1631; *Angew. Chem. Int. Ed. Engl.* **1996**, *35*, 1542–1544.
[35] D. Williams, M. Westwell, *Chem. Soc. Rev.* **1998**, *27*, 57–63.
[36] F. Cozzi, R. Annunziata, M. Benaglia, M. Cinquini, L. Raimondi, K. Baldridge, J. Siegel, *Org. Biomol. Chem.* **2003**, *1*, 157–162.
[37] R. R. Gardner, S. L. Mckay, S. H. Gellman, *Org. Lett.* **2000**, *2*, 2335–2338.
[38] B. Gung, X. Xue, H. Reich, *J. Org. Chem.* **2005**, *70*, 3641–3644.
[39] M. Sindkhedkar, H. Mulla, A. Cammers-Goodwin, *J. Am. Chem. Soc.* **2000**, *122*, 9271–9277.
[40] S. Paliwal, S. Geib, C. S. Wilcox, *J. Am. Chem. Soc.* **1994**, *116*, 4497–4498.
[41] J. Adrian, C. Wilcox, *J. Am. Chem. Soc.* **1992**, *114*, 1398–1403.
[42] E. Kim, S. Paliwal, C. S. Wilcox, *J. Am. Chem. Soc.* **1998**, *120*, 11192–11193.
[43] J. Ribas, E. Cubero, F. Luque, M. Orozco, *J. Org. Chem.* **2002**, *67*, 7057–7065.
[44] K. Nakamura, K. N. Houk, *Org. Lett.* **1999**, *1*, 2049–2051.
[45] S. Cockroft, C. Hunter, *Chem. Commun.* **2006**, 3806–3808.
[46] D. P. Curran, S. Geib, N. Demello, *Tetrahedron* **1999**, *55*, 5681–5704.
[47] S. M. Verma, N. B. Singh, *Aust. J. Chem.* **1976**, *29*, 295–300.
[48] W. R. Carroll, P. Pellechia, K. D. Shimizu, *Org. Lett.* **2008**, *10*, 3547–3550.
[49] C. Degenhardt, J. Lavin, M. Smith, K. Shimizu, *Org. Lett.* **2005**, *7*, 4079–4081.
[50] Y. S. Chong, M. D. Smith, K. D. Shimizu, *J. Am. Chem. Soc.* **2001**, *123*, 7463–7464.
[51] G. Rushton, W. G. Burns, J. M. Lavin, Y. S. Chong, P. Pellechia, K. Shimizu, *J. Chem. Educ.* **2007**, *84*, 1499–1501.
[52] W. Stewart, T. Siddall, *Chem. Rev.* **1970**, *70*, 517–551.
[53] J. Lavin, K. Shimizu, *Chem. Commun.* **2007**, 228–230.
[54] D.-S. Choi, Y. S. Chong, D. Whitehead, K. D. Shimizu, *Org. Lett.* **2001**, *3*, 3757–3760.

 © 2009 Wiley-VCH Verlag GmbH & Co. KGaA, Weinheim

[55] D. Smithrud, E. Sanford, I. Chao, S. Ferguson, D. Carcanague, J. Evanseck, K. Houk, F. Diederich, *Pure Appl. Chem.* **1990**, *62*, 2227–2236.
[56] C. A. Hunter, J. Sanders, *J. Am. Chem. Soc.* **1990**, *112*, 5525–5534.
[57] D. Hamilton, J. Davies, L. Prodi, J. Sanders, *Chem. Eur. J.* **1998**, *4*, 608–620.
[58] SPARTAN '04, Wavefunction Inc., http://www.wavefunction.com.
[59] S. Kato, T. Matsumoto, K. Ideta, T. Shimasaki, K. Goto, T. Shinmyozu, *J. Org. Chem.* **2006**, *71*, 4723–4733.
[60] A. S. Cooray, K. De Silva, *J. Mol. Struct.* **2004**, *678*, 223–231.
[61] A. Muehldorf, D. Vanengen, J. C. Warner, A. Hamilton, *J. Am. Chem. Soc.* **1988**, *110*, 6561–6562.

Received: February 20, 2009
Published online: July 31, 2009

 © 2009 Wiley-VCH Verlag GmbH & Co. KGaA, Weinheim